

Torque Production in Permanent-Magnet Synchronous Motor Drives with Rectangular Current Excitation

THOMAS M. JAHNS, MEMBER, IEEE

Abstract—Special features of torque production in self-controlled permanent-magnet (PM) synchronous motor drives with rectangular current excitation have been investigated. Addressed issues include the generation of undesired torque pulsations at low speeds and system operating locus limits imposed at high speeds by saturation of the current regulator. Attention is limited to motors in which sources of reluctance torque are suppressed by surface-mounting of the rotor magnets and skewing of the stator slots. Results from the low-speed investigation indicate that the pulsating torque can be minimized by a combination of steps including proper adjustment of the rotor magnet pole arc and effective use of rotor speed feedback compensation. High-speed saturated-regulator performance is significantly influenced by the 120 electrical degree inverter switch conduction intervals inherent with rectangular current excitation. The system torque-speed operating envelope can be expanded by several means, including on-line adjustment of the converter excitation phase angle α , but resulting performance trade-offs require careful scrutiny. A 15-kW prototype PM synchronous motor drive system has been used to confirm key analytical results.

INTRODUCTION

Background

PERMANENT MAGNET (PM) synchronous motors with power ratings greater than 5 kW have recently become subjects of growing interest for variable-speed drive systems. Such drives have already been successfully implemented in a variety of applications ranging from electric cars [1] to machine tools [2]. Several different combinations of power converter configurations and motor control strategies have been reported in the literature for obtaining high performance from three-phase PM synchronous motors [3], [4]. Torque is typically controlled in these systems by regulating the amplitudes of the motor phase currents which are synchronized in phase with the instantaneous rotor position.

One excitation scheme for PM synchronous motors which has proven particularly attractive for higher power drive systems consists of three-phase motor excitation with rectangular (quasi-square wave) current waveforms. This excitation can be conveniently delivered with a two-stage power converter configuration shown schematically in Fig. 1. As shown, this converter consists of a cascade connection of a three-phase full-bridge inverter and a two-quadrant switching current regulator. Each of the six controlled inverter switches conducts motor current for 120 electrical degrees ($^{\circ}$ elec) per cycle. Since these conduction intervals are synchronized with the rotor position,

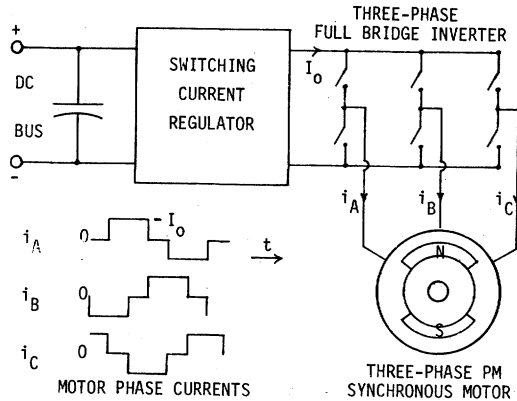


Fig. 1. Basic rectangular current drive power circuit.

the inverter is serving as an electronic equivalent of the mechanical commutator in a conventional dc motor. The switching current regulator stage which precedes the inverter regulates the amplitude of the applied motor current I_0 during both motoring and braking operation.

Attractive features of this approach include the resulting simplicity of inverter phase sequencing, the low switching frequency demands on the inverter switches, and the ease of achieving torque control by regulating the inverter input current. However, adoption of the rectangular current excitation scheme has a direct impact on the torque production characteristics of the PM synchronous motor which deserves the consideration of the drive system designer. These effects are typically most significant at the two extremes of the speed operating range—at very low speeds during positioning operations and at high speeds when the converter is delivering its maximum available output power.

For positioning applications, interaction of the nonsinusoidal phase currents and air-gap magnetic flux distribution can give rise to torque pulsations which become particularly objectionable at low speeds. Since most electric machines have been designed for sinusoidal excitation, optimization of PM synchronous machine design for nonsinusoidal converter excitation has received little attention in the literature. Recently presented work suggests the use of concentrated stator windings to achieve performance improvements [5], [6], but the presence of unskewed stator slots generates cogging reluctance torque components which remain even when the stator coils are unexcited. Nevertheless, rotor magnet geometry and dimensions do provide design degrees of freedom for drive performance improvements which are unavailable with other types of ac machines.

High-speed torque limits for the PM synchronous motor are determined by degradation of the converter's ability to develop

Paper IPCSD 83-54, approved by the Industrial Drives Committee of the IEEE Industry Applications Society for presentation at the 1983 Industry Applications Society Annual Meeting, Mexico City, Mexico, October 3-7. Manuscript released for publication October 22, 1983.

The author is with the General Electric Company, Research and Development Center, Building 37-325, P.O. Box 43, Schenectady, NY 12301.

current in the motor phases as the line-to-line back-EMF motor voltage approaches the inverter source voltage. As the speed increases, the current regulator stage in the drive configuration of Fig. 1 becomes saturated in its full "on" state, applying the low-impedance source voltage to the inverter input bus. However, the fixed 120° elec conduction intervals of the inverter switches distinguish this system from the more conventional 180° conduction "six-step" voltage-source inverter drive. Although a comparison of the effects of 120° and 180° conduction intervals on induction motor operation has been presented [7], the system high-speed performance implications of 120° conduction have not been as thoroughly discussed for the PM synchronous motor. The resulting system torque-speed operating envelope is strongly influenced by several factors which deserve attention, including the machine design and converter excitation control algorithm.

Scope of Present Work

The purpose of this paper is twofold: first, to investigate the nature of low-speed torque pulsations in rectangular current PM synchronous motor drives leading to techniques for its reduction through improved motor and controller design; and second, to investigate drive system performance limits at high speeds in order to identify techniques for achieving extended high-speed operating ranges.

The range of PM synchronous motor designs considered in this investigation is limited to machines with nonsalient stator and rotor iron structures. This constraint on rotor construction is satisfied most readily with ceramic or rare-earth permanent magnets mounted on the surface of a cylindrical iron rotor core [8]. Using this construction, a radial air-gap magnetic flux distribution is developed without the iron saliency associated with interior-magnet configurations [9]. Stator slots (or, equivalently, rotor magnets) are assumed to be skewed by one slot pitch in order to eliminate the reluctance torque effects which are otherwise present. In addition, the rotor is assumed to be designed without any type of damper winding.

Considered converter configurations include those in which the inverter switches in Fig. 1 are turned off (commutated) at will without the need for large capacitors across the terminals of the motor. Thus the conventional autosequential commutated inverter (ASCI) configuration is not addressed in this investigation. In the absence of these commuting capacitors, it is assumed that the inverter includes free-wheeling diodes to circulate motor reactive currents following the openings of the inverter switches. For purposes of generality, details of the converter current regulator algorithm will be avoided in these discussions by means of appropriate analysis simplifications.

LOW-SPEED TORQUE PRODUCTION

Simplified Motor Model Definition

Pulsating torque generation in rectangular current PM synchronous motor drives is strongly influenced by motor parameter selection. In particular, dimensions of the rotor permanent magnet poles play a key role in determining the motor's torque production characteristics. Detailed torque calculations for such machines typically require extended finite element analy-

ses to model magnetic flux distributions accurately including nonlinear effects such as localized iron saturation. However, considerable insight into the torque production mechanism and parameter dependencies can be gained by employing a simplified linear model.

A developed Cartesian axial view of the motor construction adopted for this analysis is shown in Fig. 2. As illustrated in this figure, it is assumed that the three stator phases occupy consecutive nonoverlapping 60° elec phase belts along the stator air-gap surface. Assuming that the number of stator slots per pole per phase is an integer and that the stator slots are skewed by one slot pitch as noted in the preceding section, the surface current density distribution can be modeled as spatially uniform along each excited segment of the air-gap periphery. All stator slot effects are ignored.

For the rotor, the simplified model assumes that the surface permanent magnets contribute a purely radial magnetic flux density distribution which can be modeled as shown in Fig. 2. By adopting this axially independent trapezoidal model, the effects of varying degrees of flux fringing can be conveniently represented in this analysis. The modeled shape of this flux density distribution is consistent with the reported results of previous finite-element analyses for this type of motor construction [10]. Since the incremental permeability of ceramic and rare-earth magnets is approximately that of air, the effective air-gap length is assumed to be constant at all rotor positions. All of the machine iron is modeled as infinitely permeable with no magnetic saturation effects.

Taken together, these assumptions provide a simplified motor model in which net shaft torque is contributed only by the interaction of the permanent magnet flux density distribution of Fig. 2 and the instantaneous phase currents. Empirical evidence gathered during the course of this investigation supports the validity of these assumptions for obtaining insights into machine operation, at least for nominal operating conditions.

Ideal rectangular current wave excitation has been assumed for this analysis (Fig. 1). That is, high-frequency current ripple contributed by the current regulator stage is ignored, along with finite di/dt limits imposed by the motor phase inductances. These assumptions are consistent with the low-frequency operating points considered in this analysis. The stator phase currents are synchronized with the instantaneous rotor position to produce maximum average torque/A, such that the net stator current vector is, on average, in space quadrature with the rotor flux vector. In terms of the Fig. 2 model, this implies that each phase belt section conducts constant current for 120° elec of rotor movement per half-cycle, beginning when the center of the phase belt is 60° elec advanced from the center of the approaching rotor pole. Thus, for the conditions shown in Fig. 2, the rotor position corresponds to the current transition point from phase C to phase A.

Torque and Back-EMF Calculations

The motor model introduced earlier provides the basis for straightforward calculation of the instantaneous motor torque waveform during rectangular current excitation, as well as the back-EMF waveform induced in each stator phase by the rotating rotor magnets. These key motor variables can be calculated

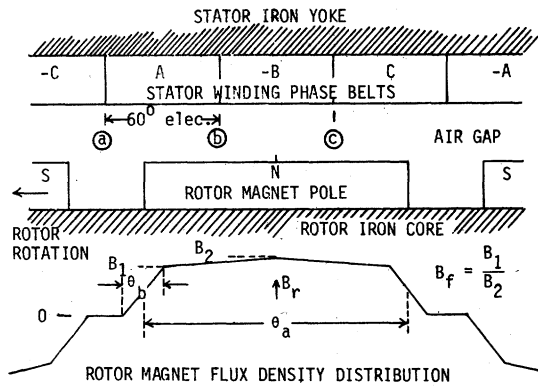


Fig. 2. Developed axial view of PM motor including model for magnet radial flux density distribution.

either by differentiating the net coil flux couplings according to the coenergy method, or by integrating the Lorentz force density ($J \times B$) along each of the individual coil sides [11]. Constant rotor speed is assumed throughout this analysis. Although details of these derivations will not be presented here, either calculation method leads to results which can be simplified into the following forms:

$$T_e(t) = 4qrl_m(N_p I_p)B_{ave2}(t) \quad (1)$$

$$V_b(t) = 2N_p r l_m \omega_m B_{ave1}(t) \quad (2)$$

where

$T_e(t)$ instantaneous value of the motor shaft torque (neglecting friction and windage) during rectangular current excitation;

$V_b(t)$ instantaneous value of the rotor-induced back-EMF in the selected stator phase assuming parallel connection of the q pole-pair stator coil sets;

$B_{ave2}(t)$ instantaneous spatial average value of the rotor PM flux density averaged over the 120° elec span of the two conducting stator phase belts within each pole pitch, e.g., for Fig. 2 with phases A and B excited,

$$B_{ave2} = \frac{3}{2\pi} \int_a^c B_r(\theta) d\theta;$$

$B_{ave1}(t)$ instantaneous spatial average value of the rotor PM flux density averaged over the 60° elec phase belt of the selected phase; for phase A in Fig. 2,

$$B_{ave1} = \frac{3}{\pi} \int_a^b B_r(\theta) d\theta.$$

(Additional variable definitions are presented in the Nomenclature at the end of this paper.)

Fig. 3 presents typical computer predicted waveforms for the unexcited stator phase back-EMF and the developed shaft torque during rectangular current excitation. Motor parameters used in this analysis were taken from a 100-Nm prototype PM synchronous motor tested in the laboratory. Specifications of this machine are provided in the Appendix. The rotor magnet

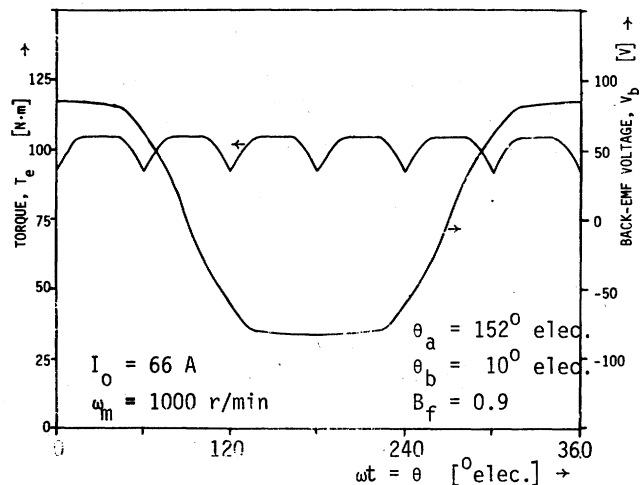


Fig. 3. Calculated motor torque and back-EMF waveforms.

flux density distribution has been modeled as shown in Fig. 2, with θ_a matching the actual rotor magnet pole arc of 152° elec and θ_b and B_f adjusted to reflect the influence of rotor flux fringing.

Although it has not been possible to measure the instantaneous shaft torque waveform for the prototype drive system, the validity of the simplified motor model has been partially tested by measuring the rotor-induced back-EMF waveform in the unexcited stator phases. Fig. 4 provides an oscilloscope of the measured back-EMF waveform for the prototype motor which matches the predicted waveform within a few percent at all points.

Torque Production Dependence on Rotor Magnet Dimensions

The dominant harmonic component in the Fig. 3 pulsating torque waveform occurs at six times the fundamental excitation frequency, corresponding to the six inverter switch conduction intervals per cycle. In fact, each pronounced dip in the motor torque occurs in the immediate vicinity of an inverter switch event as each rotor magnet in Fig. 2 gradually shifts its alignment to the newly conducting phase belt from the offgoing segment.

The simplified motor model defined in the preceding section has been exercised to determine the dependence of average and pulsating torque production on rotor magnet pole arc and flux fringing characteristics. Figs. 5 and 6 present plots of average and pulsating torque components, respectively, as a function of rotor magnet pole arc, with the magnet end fringing angle θ_b varied to produce a family of curves. The pulsating torque component has been quantized by integrating the difference between the instantaneous torque and the average torque, providing a variable T_{pi} , which is proportional to the estimated peak-to-peak speed pulsation. Assuming that the rotating load is stiffly coupled to the drive motor with equal inertia, a T_{pi} value of 0.01 Nm·s corresponds roughly to a peak-to-peak rotor speed pulsation of 1 r/min for the prototype system (i.e., $\Delta\omega_m$ (r/min) = $T_{pi}/J_t = 100 T_{pi}$ (Nm·s)). The average torque curves have been normalized using the T_{ave} value for $B_f = 1.0$ and $\theta_a = 180^\circ$ elec as base torque. Key observations drawn from these

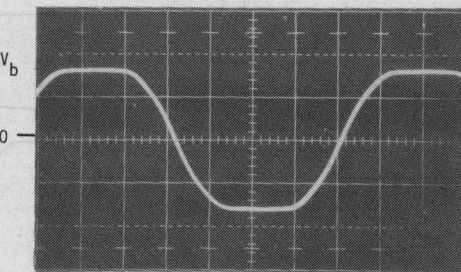


Fig. 4. Measured prototype motor back-EMF. 1000 r/min; vertical: 50 V/div; horizontal: 2 ms/div.

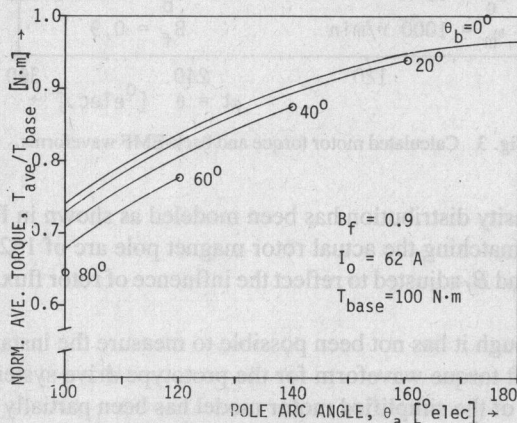


Fig. 5. Calculated normalized T_{ave} as function of magnet flux density distribution parameters.

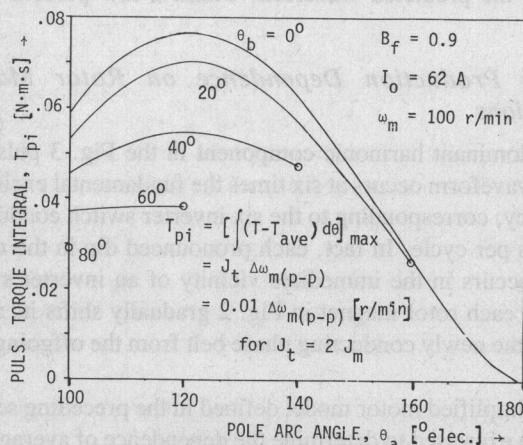


Fig. 6. Calculated pulsating torque integral T_{pi} as function of flux density distribution parameters.

curves include the following.

- Average torque will be maximized and pulsating torque simultaneously minimized by increasing the magnet pole arc angle θ_a as much as possible.
- Increased rotor flux fringing (either by increasing θ_b or by decreasing B_f) has the effects of reducing average torque and pulsating torque for any fixed value of magnet pole arc angle θ_a .
- Choosing a rotor magnet pole arc of 120° elec has the adverse effect of maximizing pulsating torque production for rectangular current excitation.

These observations must be tempered by practical limits on the ranges of achievable motor parameter values. Most significantly, the limit of 180° elec rotor magnet pole arc with no flux fringing is unachievable in practice due to the unavoidable flux shunting between adjacent butted pole pieces. Recognition of this limit does not conflict with the desirability of designing the rotor magnets so that the crestwidth of the rotor flux distribution in Fig. 2 approaches 180° elec for minimum pulsating torque production. However, since this limit can only be approached but not reached, Fig. 6 suggests that complete elimination of the pulsating torque component for ideal rectangular current excitation cannot be achieved with this type of PM synchronous motor construction.

Active Converter Compensation of Pulsating Torque

Although improved design of the PM synchronous motor represents an appealing approach for minimizing pulsating torque effects, further reductions are possible by appropriately adjusting the current excitation waveform. In particular, the rotor speed feedback signal which is typically used in high-performance drive applications for closed-loop speed control also provides a means of actively compensating the pulsating torque component at low speeds. That is, the closed-loop speed control senses the rotor speed disturbances caused by the pulsating torque component and responds by adjusting the motor current to counteract these disturbances.

The ability of the closed-loop speed control to respond to speed disturbances improves as the speed/frequency decreases because of the finite bandwidth of this loop. However, the drive-train speed becomes increasingly sensitive to the effects of pulsating torque at low speeds because of the integrating nature of the basic torque-speed relationship. The extent to which the speed controller dynamics dominate low-speed torque production determines the effectiveness of this compensation technique.

To explore this issue, a small-signal linearized model of the PM synchronous motor drive system has been developed which includes the rotor speed feedback control loop as well as the pulsating torque production mechanism (Fig. 7). As in the case of the motor model, assumptions have been made to simplify the model while preserving its basic integrity. Although a detailed derivation of this model will not be presented here, a short discussion follows to note its key features and establish its plausibility.

Those familiar with the modeling of conventional dc servo control loops will note the similarity of the PM synchronous motor model in Fig. 7 to that of the standard dc servo motor. This is possible since, as noted previously, the inverter plays the same role as the mechanical commutator in the dc motor, making the inverter bus terminals essentially equivalent to the dc motor terminals for control loop modeling [16]. The switching current regulator stage is modeled as a simple linear current regulator loop with a proportional gain, a reasonable model since the ratio between the frequency bandwidths of the current and speed loops is typically quite high (≥ 10). A proportional-integral (P-I) controller has been adopted for the speed regulator model, and the mechanical drive-train has been modeled using a very simple first-order model.

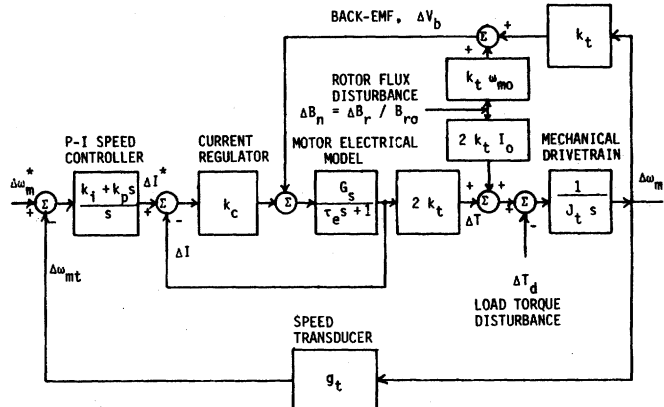


Fig. 7. Linearized drive system model for analysis of pulsating torque feedback compensation.

The preceding motor analysis results in (1) and (2) have shown that variations in the motor torque and rotor-induced back-EMF during each sixth-cycle of excitation are produced by the periodic pulsations of the B_{ave} terms contributed by the rotor magnet flux density distribution. These key nonlinear effects have been included in the Fig. 7 model by, effectively, transforming the ac motor model into the synchronous rotating reference frame and then linearizing about the desired operating point. The resulting ΔB_n disturbance input, representing the normalized variation of the B_{ave} term about its nominal operating point, is the source of both the pulsating torque production and the pulsations in the stator back-EMF voltage appearing at the inverter bus terminals. All of the frequency components in the ΔB_n disturbance signal occur at multiples of six times the excitation frequency; that is, at $(6nq\omega_{mo})$, where $n = 1, 2, \dots$

The linearized model of Fig. 7 provides the basis for deriving the desired transfer function relating the shaft speed pulsations $\Delta\omega_m$ to the periodic ripple in the normalized rotor flux density ΔB_n . This transfer function is presented below for a given operating point bus current I_o , shaft speed ω_{mo} , and rotor flux density level B_{ro} (which sets the torque constant k_t):

$$\frac{\Delta\omega_m}{\Delta B_n} = \frac{2k_t s(a_1 s + a_0)}{b_3 s^3 + b_2 s^2 + b_1 s + b_0} \quad (3)$$

where

$$\begin{aligned} a_0 &= I_o(1 + k_c G_s) - k_t G_s \omega_{mo} \\ a_1 &= I_o \tau_e \\ b_0 &= 2k_t k_c k_i G_s g_t \\ b_1 &= 2k_t G_s(k_t + g_t k_c k_p) \\ b_2 &= J_t(1 + k_c G_s) \\ b_3 &= J_t \tau_e \end{aligned}$$

A plot of the transfer function amplitude as a function of disturbance frequency (Fig. 8) provides insights into the effectiveness of this compensation technique. The P-I speed controller parameters have been adjusted to provide critically damped response with a bandwidth of 200 rad/s, reflecting the adjusted performance of the prototype system. Fig. 8 also includes, for comparison, a plot of this same transfer function with the speed

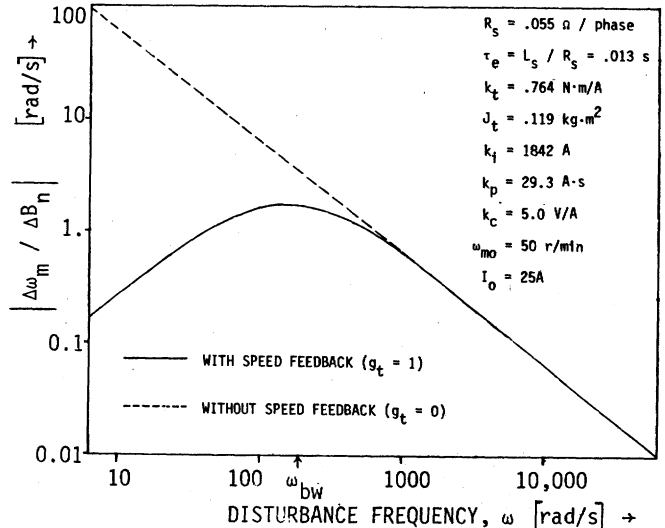


Fig. 8. Calculated magnitude plots for $\Delta\omega_m/\Delta B_n$ with and without speed feedback.

loop opened ($g_t = 0$), deactivating the pulsating torque compensation loop. Operating point and parameter values are summarized in Fig. 8.

The Fig. 8 curves indicate that the closed-loop speed control will act to attenuate the open-loop speed pulsation provided that the frequency of the dominant pulsating torque component at $(6q\omega_{mo})$ is lower than the bandwidth of the speed loop ω_{bw} . In fact, Fig. 8 indicates that the peak pulsating speed amplitude in the closed-loop system occurs at an operating point rotor speed of $\omega_{mo} = \omega_{bw}/(6q)$; the relative attenuation of the speed pulsation increases rapidly (proportional to $(\omega_{mo}/\omega_{bw})^2$) as the operating speed is lowered below this threshold. Closer inspection of the $\Delta\omega_m/\Delta B_n$ transfer function indicates that the operating point speed has only a weak effect on the shape and amplitude of the Fig. 8 closed-loop curve for a wide range of operating conditions. On the other hand, the transfer function amplitude is nearly linearly proportional to operating point current I_o .

Tests have been conducted with the prototype PM synchronous motor drive system to verify empirically the attenuating effect of closed-loop speed control on the rotor speed pulsation. Oscillograms presented in Fig. 9 provide a direct comparison of the resulting rotor speed pulsation with the speed feedback loop opened and closed. Also provided are phase current waveforms which demonstrate the effect of the speed loop in adjusting the instantaneous current to achieve the pulsating speed attenuation. Note that the dominant speed pulsation component at six times the excitation frequency is clearly evident in Fig. 9(a). Although a small amount of speed pulsation remains in the closed-loop speed trace in Fig. 9(b) around the switching instants, the attenuation in its amplitude compared to the open-loop case is significant.

HIGH-SPEED DRIVE SYSTEM OPERATING LIMITS

Nature of Saturated Current Regulator Operation

Active current regulation during motoring operation demands the availability of a net positive voltage difference between the source voltage and instantaneous line-to-line rotor-

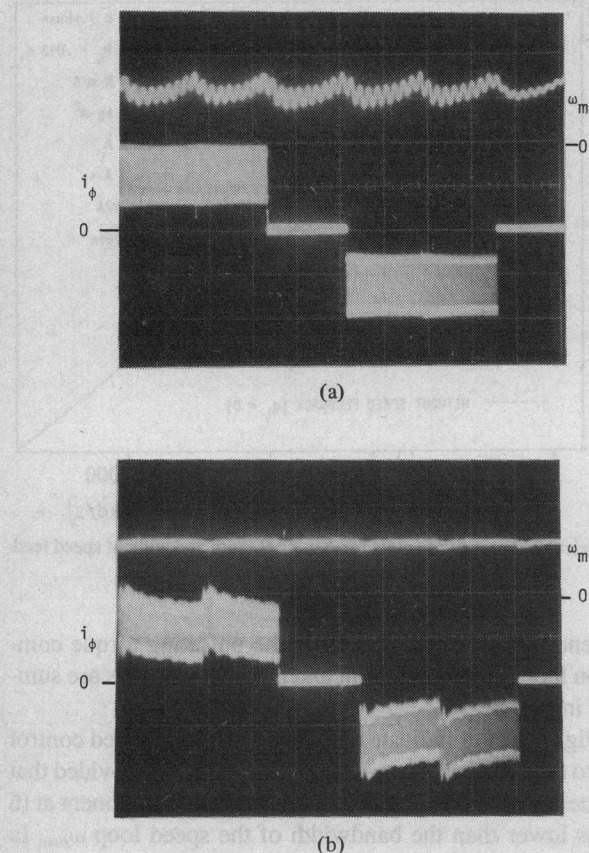


Fig. 9. Measured rotor speed (ω_m) and stator phase current (i_ϕ) showing effects of speed feedback. Vertical: $\omega_m = 30$ (r/min)/div; $i_\phi = 20$ A/div; horizontal: 50 ms/div. (a) Without speed feedback. (b) With speed feedback.

induced back-EMF to drive the motor phase currents. Since the amplitudes of the back-EMF waveforms are proportional to rotor speed, the available driving voltage shrinks to zero as the speed is increased, thereby preventing the current regulator from performing its role at high speeds. The resulting current error causes the current regulator to saturate in the "full on" condition, giving the system many characteristics of a voltage-source inverter (VSI) drive in this operating regime. Details of the transition from nominal rectangular-current operation to saturated-regulator operation have been avoided in this investigation by considering only the limiting operating regime with the current regulator fully saturated, which is common to all such systems at high speeds.

Since the two switches in each inverter leg conduct for a total of 240° elec during each cycle, there are two 60° intervals per cycle when the motor terminal voltage is not directly constrained by the source voltage V_s , as shown in Fig. 10. If any current flows in the motor phase during these intervals due to reactance effects or back-EMF-induced circulating currents, the associated freewheeling diodes force the terminal voltage to the positive or negative bus potential, depending on current polarity. On the other hand, when the motor phase current drops to zero during these intervals, the motor terminal voltage is free to assume any voltage level between the two bus potentials, depending on internal motor voltage drops.

As noted in [12], the phase angle between the switching instants of the inverter switches and the instantaneous rotor position plays a very significant role in determining the saturated-

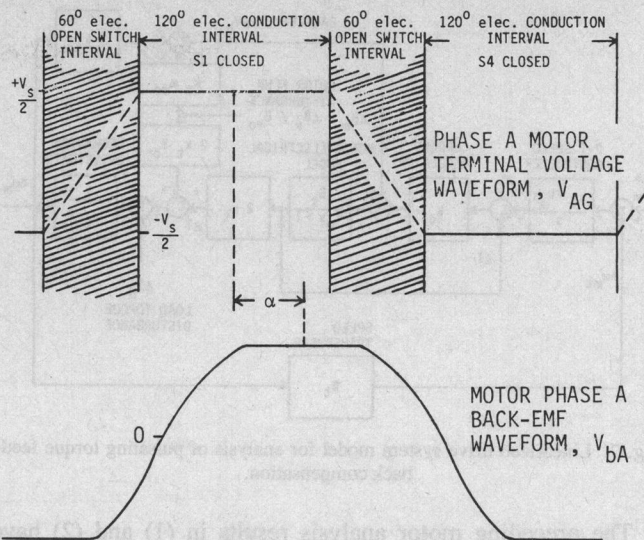


Fig. 10. Motor phase A voltage waveforms during high-speed saturated-regulator operation.

regulator performance characteristics. This excitation phase shift angle α has been defined as shown in Fig. 10, such that α is zero when the 120° elec inverter switch conduction intervals are in phase with the back-EMF voltage induced in the associated motor phase. At low speeds while the current regulator is active, α is held at zero to develop maximum torque/A.

Drive Simulation for Saturated-Regulator Operation

Performance characteristics of the PM synchronous motor drive system during saturated-regulator operation have been analyzed by simulating the drive system on a digital computer. Advantages of this approach include the flexibility of the resulting simulation model for investigating transient and steady-state drive operation at all speeds, including low speeds when the current regulator is active.

Fig. 11 provides a schematic of the simulated drive configuration, consisting of the PM synchronous motor, a fixed voltage source (V_s), six inverter switches (S1-S6), six freewheeling diodes (D1-D6), and a regulator switch (S7). Note that no external inductors are included in this model since it is assumed that S7 can switch fast enough to regulate the current working with only the motor phase inductances. During saturated-regulator operation, S7 is controlled to be constantly closed. Each motor phase has been modeled as a back-EMF voltage source (V_b) in series with a resistance (R_b) and inductance (L_b). Although simple, this motor model is adequate for this system simulation since the considered motor construction has no net rotor saliency or damper windings.

This simulation has been carried out using the so-called "constant topology" approach [13] in which each converter switching device and diode is modeled by a time-varying resistance. The value of each such resistance switches between high- and low-impedance values repeatedly during the simulation depending on the conduction state of the associated switch. Since details of this simulation technique have been provided by Nehl *et al.* [14], only a brief description of this method is presented here.

Waveforms for all of the drive variables are calculated by

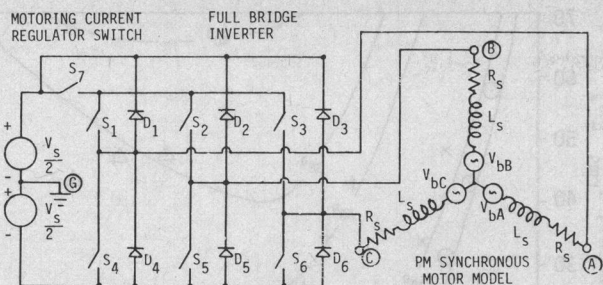


Fig. 11. Simulation drive power circuit schematic.

assuming that the system can be analyzed as a linear constant coefficient system for short intervals of time. On this basis, the system matrix exponential is calculated at each time instant in order to increment all of the drive voltages and currents ahead one time step, at which point all of the switch and diode conduction states are reevaluated. Motor back-EMF waveforms are provided to the simulation as inputs, generated for the motor of interest by the motor analysis program described in the first section of this paper. Rotor speed is held constant throughout each simulation, and inverter switch conduction states are synchronized with the instantaneous rotor position according to Fig. 10.

Simulation inputs include all of the drive circuit parameters in Fig. 11, along with the rotor speed ω_m and excitation phase angle α . In order to calculate steady-state performance, each simulation is allowed to proceed until all transient modes decay sufficiently, and then the operating point performance variables including torque and current amplitude are calculated.

Prototype PM Synchronous Motor Drive

System parameters of a prototype PM synchronous motor drive tested in the laboratory have served as the basis for many of the quantitative results presented in this paper. The prototype machine is rated at 100 Nm, producing 15.7 kW at 1500 r/min. Although the parameters of this machine reflect its power rating and specific design, it is representative of the type of PM synchronous motor construction addressed in this investigation. Key machine parameter data are summarized in the Appendix.

The prototype power converter used to excite this machine consists of six inverter thyristor switches preceded by a transistorized switching current regulator stage, according to the block diagram in Fig. 1. These transistors play the dual roles of regulating the inverter bus current and force-commutating the inverter thyristors, with independent commutation of the upper and lower inverter leg devices. Nominal converter input bus voltage is 280 V dc, and the steady-state converter power rating is 15 kW, which is compatible with the prototype motor rating. A photo of this prototype drive system is provided in Fig. 12.

Steady-State Performance Characteristics during Saturated-Regulator Operation

The system designer must balance several system parameters in order best to achieve the drive high-speed performance specifications. These parameters include motor equivalent circuit parameters, converter source voltage, and adjustment of the inverter/rotor phase angle synchronization. Effects of these system parameters on drive performance in the saturated-regulator

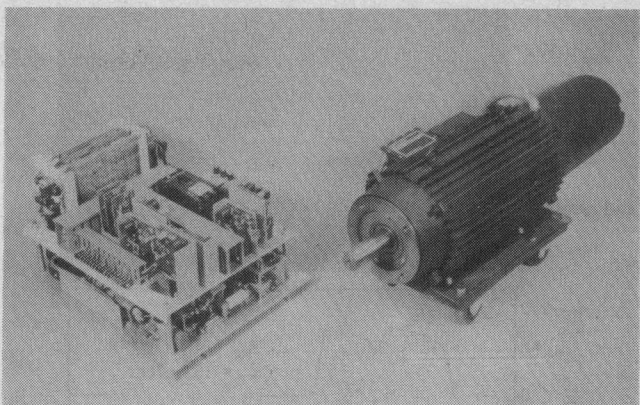


Fig. 12. Prototype 15-kW power converter and motor.

operating regime have been explored using the drive simulation program described earlier, using parameters of the prototype system as a base. The simulation program has demonstrated its ability to predict accurately the performance of the prototype system in several ways, including good correlation of predicted and measured drive waveforms. A sample comparison is provided in Fig. 13 for one typical operating point.

Figs. 14–17 provide plots of calculated saturated-regulator performance characteristics of the prototype drive system as a function of speed, with excitation phase angle α varied to produce families of curves. Plotted torque production characteristics include the average torque T_{ave} in Fig. 14, and the pulsating torque integral T_{pi} in Fig. 15, which, as explained in an earlier section, is proportional to the peak-to-peak rotor speed pulsation. The family of average torque curves indicates that the drive torque-speed operating locus can be expanded considerably by adopting a control algorithm which increases the excitation angle α in the high-speed regime. For example, the maximum speed at which 50 Nm (0.5 rated torque) can be developed increases from 1400 r/min to 2000 r/min as α is adjusted from 0 to 40° elec. At any given speed, the average torque becomes increasingly sensitive to α as the value of α increases.

As shown in Fig. 15, increases in α which raise the average torque are accompanied by significant increases in the pulsating torque and hence pulsating speed characteristics, particularly as α increases beyond 15° elec. Although all of the T_{pi} curves fall with speed, the ratio of T_{pi} to T_{ave} at a given speed tends to rise as α is increased. This rise in T_{pi} is particularly large as α increases from 15° to 30°.

Fig. 16 shows that the dependence of rms phase current I_{rms} on excitation phase angle α is similar to that of the average torque in Fig. 14, although I_{rms} rises at high speed for $\alpha \geq 30^\circ$. The ratio of T_{ave}/I_{rms} as a function of motor speed and α is presented in Fig. 17, providing insight into how effectively the converter's current capacity is being used at each operating point. For speeds below 1400 r/min, the T_{ave}/I_{rms} ratio exhibits a maximum value of 1.87 Nm/A for an excitation angle of 15°, representing the operating conditions for which the phase current fundamental component is most nearly in phase with the back-EMF waveform. For higher speeds, the value of α providing the highest T_{ave}/I_{rms} ratio increases, reflecting increases in the motor phase reactances. However, note that T_{ave}/I_{rms} values drop quite significantly as the speed is increased, placing higher demands on the converter.

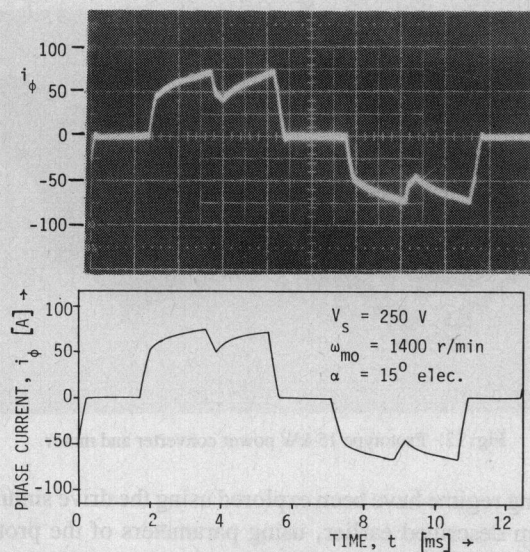


Fig. 13. Measured and calculated stator current waveforms during saturated-regulator operation.

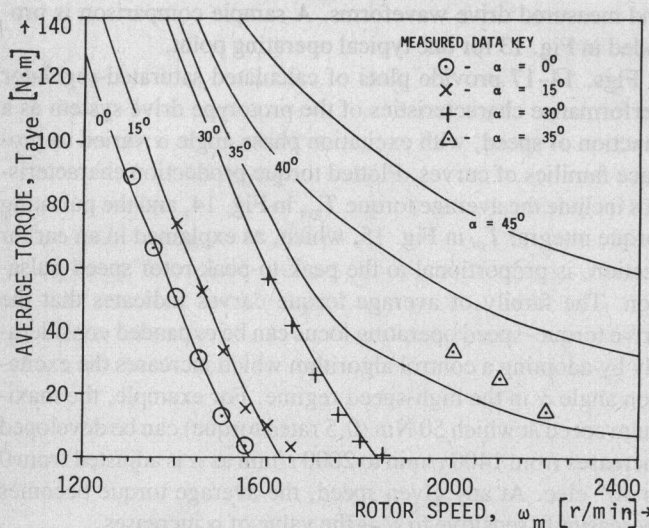


Fig. 14. Calculated and measured T_{ave} as function of rotor speed and excitation angle. $V_s = 250 \text{ V}$.

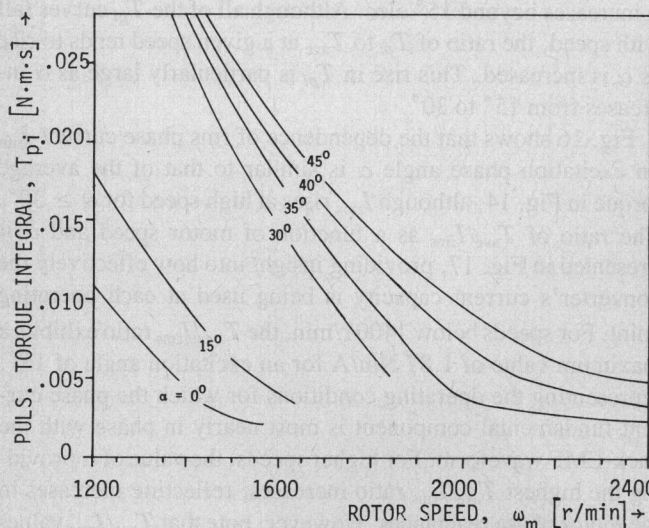


Fig. 15. Calculating pulsating torque integral T_{pi} as function of ω_m and excitation angle. $V_s = 250 \text{ V}$.

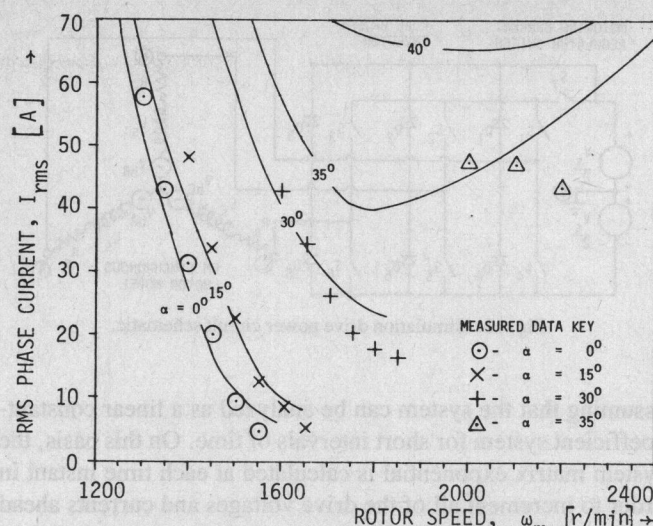


Fig. 16. Calculated and measured rms current as function of ω_m and excitation angle. $V_s = 250 \text{ V}$.

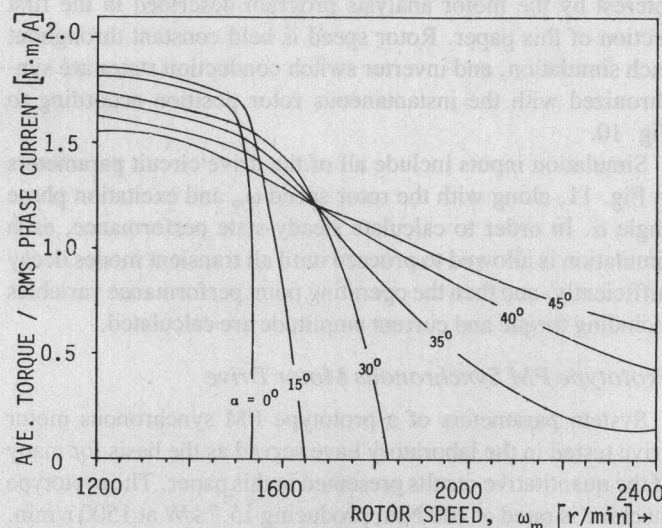


Fig. 17. Calculated torque/current ratio as function of rotor speed and excitation angle. $V_s = 250 \text{ V}$.

Empirical average torque and rms phase current data gathered for the prototype system are plotted together with the calculated curves in Figs. 14 and 16. Agreement between the measured and empirical data is generally quite good, particularly for the lower speeds and lower values of α . Remaining errors are attributed to a combination of factors, including motor parameter identification errors, and parasitic excitation phase shifts at higher speeds.

Performance Dependence on System Parameters

Having examined in some detail the saturated-regulator performance characteristics of the prototype drive system as a base, the investigation was expanded to explore the dependence of these characteristics on key system parameters. Availability of the drive simulation program makes it possible to vary each of these parameters independently over a wide range in order to isolate their individual effects. Used in this manner, the simulation program becomes a powerful tool to facilitate drive design optimization for this drive configuration.

Considerable attention has been devoted to exploring the ef-

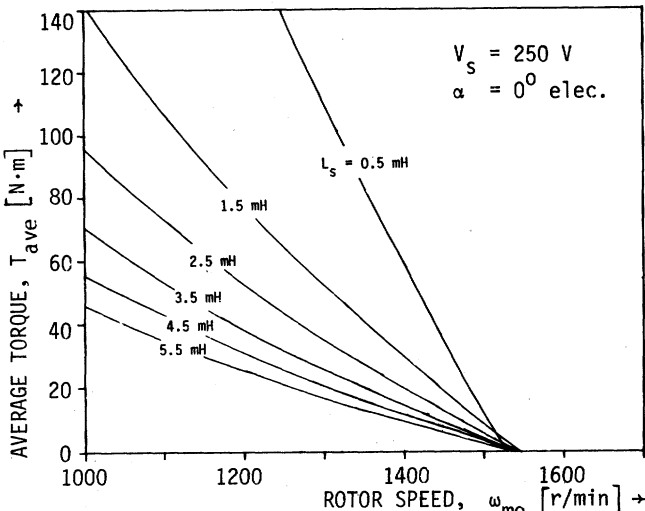


Fig. 18. Calculated T_{ave} as function of rotor speed and inductance L_s . Prototype drive parameters.

fects of motor equivalent circuit parameters on performance characteristics. For example, Fig. 18 shows the effects on average torque of increasing the motor phase inductance from 0.5 mH to 5.5 mH in several steps. Such dramatic changes in inductance might, for example, reflect stator winding changes accompanying replacement of rare-earth rotor magnets with ceramic magnets operating at lower flux densities. The Fig. 18 curves indicate that the average torque at any speed decreases as the phase inductance is raised, although the speed axis intercept for $T_{ave} = 0$ remains virtually constant at 1550 r/min. Torque pulsation curves are similarly depressed, and the T_{ave}/I_{rms} ratio increases as the inductance is raised, particularly for higher values of excitation phase angle α . Raising the motor phase resistance R_s , likewise tends to depress both the average and pulsating torque amplitudes, although the performance sensitivity is not as high as for changes in the inductance. The T_{ave}/I_{rms} ratio is adversely affected by increases in resistance for $\alpha \geq 0^\circ$.

The effects of varying the number of stator turns per phase belt coil N_p for a given motor design have also been examined. For a given stator slot size and fill factor, changing N_p will simultaneously scale L_s and R_s by a factor proportional to $(N_p)^2$, as well as scaling the back-EMF V_b linearly with N_p . It is convenient to adopt the turns factor ratio, $TF = N_p/N_b$ as the varied parameter, where N_b is the stator turns per coil of the base machine. Fig. 19 provides a set of curves which illustrate the potency of the turns factor in varying the torque-speed operating locus. However, expansion of this locus by decreasing the stator turns comes at the price of lower T_{ave}/I_{rms} ratios, which will tend to increase the converter switch current ratings. Increasing the source voltage V_s has a similar effect in expanding the torque-speed locus, although the converter trade-offs now primarily involve device voltage ratings, since motor T_{ave}/I_{rms} levels are unaffected.

Comparison of Saturated-Regulator Performance with 120° and 180° Conduction Intervals

As noted earlier, the 120° elec inverter switch conduction intervals associated with the rectangular current converter distinguish this system from many other drive configurations. For example, converters with sinusoidal PWM current regulators

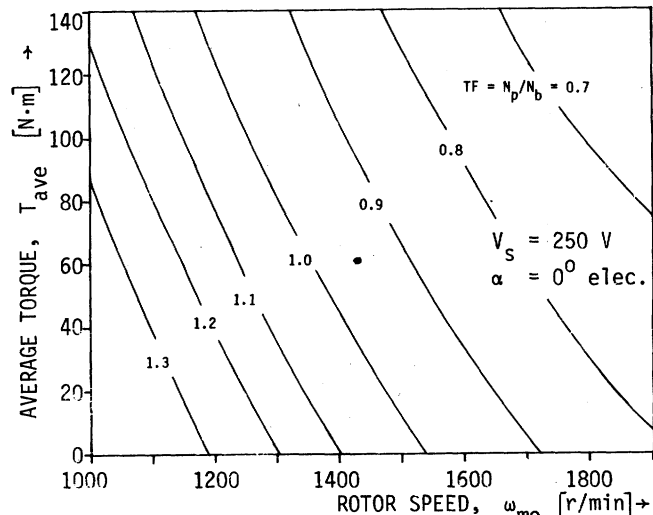


Fig. 19. Calculated T_{ave} as function of rotor speed and stator coil turns factor TF. Base prototype drive parameters for TF = 1.0.

saturate with 180° conduction intervals, delivering familiar six-step voltage waveforms to the machine at high speeds. Since the properties of six-step excitation are well-known, useful comparisons can be drawn between the PM synchronous motor performance characteristics with 120° and 180° conduction intervals.

Analysis of the 180° conduction case is simplified by the fact that the voltage excitation waveforms for each motor phase are defined at all times in terms of the bus voltage V_s . For example, the equation for T_{ave} can be conveniently expressed in closed-form, using the same motor equivalent circuit parameters as for the 120° conduction case [15]. Assume that the definition of the excitation advance angle α is a logical extension of the Fig. 2 definition for the 120° case; that is, α is zero when each 180° conduction interval is in phase with the rotor-induced back-EMF of the associated motor phase. Then,

$$T_{ave} = \frac{3V_{br}[(V_{sr} \cos \alpha - V_{br})R_s + V_{sr}X_s \sin \alpha]}{[R_s^2 + X_s^2]\omega_m} \quad (4)$$

where

$$V_{sr} = \frac{\sqrt{2}}{\pi} V_s$$

$$X_s = q\omega_m L_s.$$

However, closed-form expressions for the other important performance characteristics such as the pulsating torque are more cumbersome since they depend principally on the excitation harmonics. Given the availability of the drive simulation computer program developed for the 120° conduction case, simple modifications were introduced to extend it to the 180° case. In addition to conveniently providing all desired performance characteristics, this exercise allows useful checks on the simulation accuracy through direct comparisons of simulation and closed-form expression results. The simulation program has performed very well in all such tests.

Figs. 20-22 provide direct comparisons between calculated performance characteristics of the prototype PM synchronous motor with 120° and 180° conduction. Excitation phase angle α has been varied over identical ranges for both cases. In general, system performance is superior for 180° conduction for the

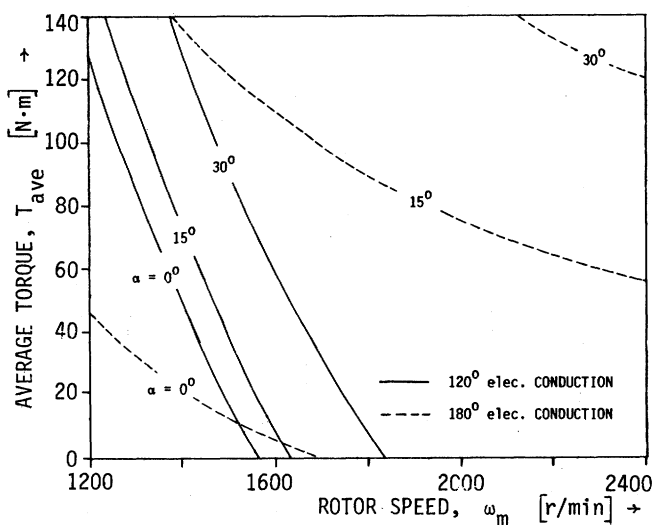


Fig. 20. Calculated T_{ave} for 120° and 180° conduction intervals as function of ω_m and α . $V_s = 250$ V.

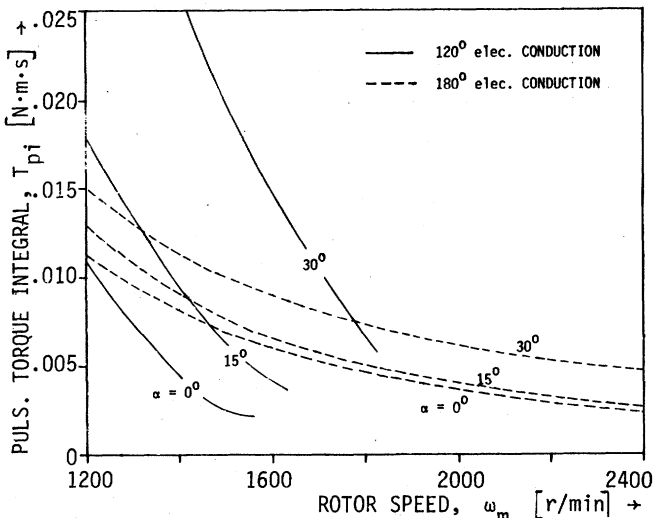


Fig. 21. Calculated T_{pi} for 120° and 180° conduction intervals as function of ω_m and α . $V_s = 250$ V.

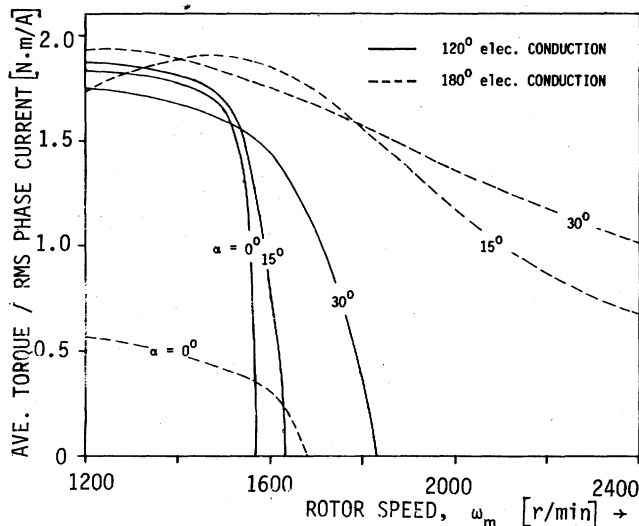


Fig. 22. Calculated torque/current ratio for 120° and 180° conduction intervals as function of ω_m and α . $V_s = 250$ V.

cases of nonzero α . For example, the torque-speed operating envelopes (Fig. 20) for $\alpha = 15^\circ$ and 30° are significantly larger when the conduction interval is 180° . Figs. 21 and 22 show that the ratios of T_{pi}/T_{ave} and T_{ave}/I_{rms} are similarly improved at high speeds with longer conduction interval for nonzero α . The relative performance advantages of 180° conduction increase as α is raised.

In contrast, these figures also show that high-speed performance is superior with 120° conduction when α is held at zero. In particular, the average torque (Fig. 20) and T_{ave}/I_{rms} ratio (Fig. 22) are significantly depressed for the longer 180° conduction interval. This difference can be very important since the simplest converter control algorithms for such drives saturate at high speeds with the excitation phase angle fixed at zero. Additional simulations of this $\alpha = 0^\circ$ case have revealed that, in contrast to the 120° conduction results, average torque with 180° conduction increases as the resistance is raised. These results are consistent with the predictions of (4) due to the dominance of the resistive term in the numerator when the excitation voltage and back-EMF waveforms are in phase ($\alpha = 0^\circ$).

Investigation of performance sensitivities to other parameters has indicated that the basic trends for 120° and 180° conduction are similar for changes in phase inductance, turns/coil, and source voltage. However, the level of sensitivity is generally higher with 180° conduction, reflecting the fixed nature of the phase excitation waveforms with 180° conduction. Since the terminal phase voltages are not directly constrained at all times with 120° conduction intervals, the motor phase voltage waveforms are free to shift in phase somewhat even though α is fixed, partially compensating for changes in parameter values.

CONCLUSION

Results have been presented for an investigation of the torque production characteristics of PM synchronous motor drives with rectangular current excitation. This drive system configuration is particularly attractive for larger drives which benefit from the reduced switching frequency of the inverter switches, as well as the simplified current regulator requirements. The investigation scope has been limited to PM synchronous motors in which sources of reluctance torque have been eliminated by surface-mounting of the rotor magnets and skewing of the stator slots or rotor magnets.

Attention has been focused on the special problems associated with drive performance in the lowest and highest speed operating regimes. Analytical results have been confirmed with empirical data gathered from a laboratory prototype 15-kW system. Key investigation results are summarized as follows.

- Under the adopted motor design constraints, low-speed pulsating torque developed with rectangular current excitation can be minimized but not entirely eliminated by designing rotor magnet pole arcs as close to 180° elec as possible, limited by flux-shunting effects between adjacent pole segments.

- A closed-loop speed regulator will act to compensate the effects of residual low-speed pulsating torque provided that the harmonic frequency presented by six times the fundamental excitation frequency falls within the bandwidth of the speed loop.

- At high rotor speeds for which the current regulator has saturated, the drive torque-speed operating locus can be ex-

panded considerably by phase shifting the inverter switch conduction intervals with respect to the rotor-induced back-EMF waveforms (excitation angle α). However, such improvements are accompanied by increases in the pulsating torque, and there are significant drops in the torque/current ratio for $\alpha \geq 30^\circ$ elec.

4) Increasing motor phase inductance has the beneficial effects of improving pulsating torque and torque/current ratio characteristics at high speeds, at the price of a smaller torque-speed operating locus. Similar trade-offs are associated with adjustments of other motor and converter design parameters in order to meet system performance requirements.

5) High-speed saturated-regulator performance characteristics developed by the rectangular current drive with 120° elec inverter switch conduction intervals are generally inferior to those provided by conventional 180° conduction (six-step voltage excitation). However, if a simple converter control algorithm is implemented which fixes the excitation phase angle α at 0° for all speeds (producing maximum torque/A at low speeds), then the saturated-regulator performance provided by 120° conduction is superior.

NOMENCLATURE

The following variables are not defined in the text.

q	Number of machine pole pairs.
r	Mid-air-gap machine radius (m).
l_m	Active stator core length (m).
N_p	Number of conductors per winding phase belt.
I_p	Current per phase-belt conductor (A).
ω_m	Rotor speed (mechanical rad/s, unless noted).
J_m	Motor rotor inertia (kg m^2).
J_t	Total drivetrain inertia ($\text{kg} \cdot \text{m}^2$).
o	As subscript, operating point value.
Δ	As prefix, incremental value about operating point.
G_s	Stator winding conductance ($= 1/R_s$) (Ω^{-1}).
B_r	Radial air-gap magnetic flux density contributed by rotor magnets (T).
V_{br}	Back-EMF rms fundamental component per phase (V).

APPENDIX

PROTOTYPE PM SYNCHRONOUS MOTOR PARAMETERS

Continuous rated torque at stall	100 Nm.
Continuous rated rms current at stall	59 A.
Back-EMF constant (per phase)	80 V(pk)/1000 r/min.
Torque constant (per phase), k_t	0.764 Nm/A.
Pole number, $2q$	8.
Rotor magnets	SmCo ₅ , 152° elec pole arc.
Stator core configuration	24 slots, skewed 15° mechanical.
Stator core length, l_m	31.5 cm.
Stator core inner diameter	12.7 cm.
Stator per-phase resistance, R_s	0.055 Ω.
Stator line-to-line inductance, $2L_s$	1.44 mH.
Rotor inertia, J_m	0.0467 kg m ² .

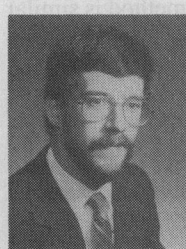
ACKNOWLEDGMENT

I wish to gratefully acknowledge the engineering staff of Gettys Motion Control Division for making available the

motor used in this investigation, as well as for many useful suggestions and discussions during the course of this work. I also thank M. Konitzer, K. Bernoteit, and F. Doran of Gould Research Center for their special efforts in fabricating the prototype converter used in this investigation.

REFERENCES

- [1] N. Demerdash, F. Lee, T. Nehl and B. Overton, "Practical application of power conditioning to electric propulsion for passenger vehicles," *IEEE Power Electronics Spec. Conf. Rec.*, 1980, pp. 211-219.
- [2] P. Zimmerman, "Electronically commutated dc feed drives for machine tools," *Drives and Controls Int.*, vol. 2, Oct./Nov. 1982, pp. 13-20.
- [3] G. Pfaff, A. Weschta, and A. Wick, "Design and experimental results of a brushless ac servo drive," *IEEE Industry Applications Soc. Conf. Rec.*, 1982, pp. 692-697.
- [4] W. Volkrodt, "Machines of medium-high rating with a ferrite-magnet field," *Siemens Rev.*, vol. 43, 1976, pp. 248-254.
- [5] T. Lipo, and F. Wang, "Design and performance of a converter optimized ac machine," *IEEE Industry Applications Soc. Conf. Rec.*, pp. 491-499, 1982.
- [6] B. Ooi, P. Brissonneau, and L. Brugel, "Optimal winding design of a permanent magnet motor for self-controlled inverter operation," *Elec. Mach. Electromech.*, vol. 6, pp. 381-389, Sept./Oct. 1981.
- [7] T. Lipo and F. Turnbull, "Analysis and comparison of two types of square-wave inverter drives," *IEEE Trans. Ind. Appl.*, vol. IA-11, Mar./Apr. 1975, pp. 137-147.
- [8] B. Sawyer, and J. Edge, "Design of a samarium cobalt brushless dc motor for electromechanical actuator applications," in *IEEE Nat. Aerospace Electronics Conf. Rec.*, 1977.
- [9] V. Honsinger, "The fields and parameters of interior type ac permanent magnet machines," *IEEE Trans. Power App. Syst.*, vol. PAS-101, pp. 867-876, Apr. 1982.
- [10] F. Fouad, T. Nehl and N. Demerdash, "Magnetic field modeling of permanent magnet type electronically operated synchronous machines using finite elements," *IEEE Trans. Power App. Syst.*, vol. PAS-100, pp. 4125-4135, Sept. 1981.
- [11] H. Woodson, and J. Melcher, *Electromechanical Dynamics, Part I: Discrete Systems*. New York: Wiley, 1968.
- [12] T. Nehl, F. Fouad, and N. Demerdash, "Digital simulation of power conditioner-machine interaction for electronically commutated dc permanent magnet machine," *IEEE Trans. Magn.*, vol. MAG-17, pp. 3284-3286, Nov. 1981.
- [13] H. Foch, B. Trannoy, and J. Faucher, "Complete simulation of a static converter by digital and analogue methods," in *Proc. 1st IFAC Symp., Control in Power Electronics and Drives*, vol. 1, 1974, pp. 363-373.
- [14] T. Nehl, F. Fouad, and N. Demerdash, "Dynamic simulation of radially-oriented permanent magnet type electronically operated synchronous machines with parameters obtained from finite element field solutions," *IEEE Trans. Ind. Appl.*, vol. IA-18, pp. 172-182, Mar./Apr. 1982.
- [15] A. Fitzgerald, C. Kingsley, and S. Umans, *Electric Machinery*, 4th ed. New York: McGraw-Hill, 1982, p. 329.
- [16] A. Jacobowicz, M. Nougaret, and R. Perret, "Simplified model and closed-loop control of a commutatorless dc motor," *IEEE Trans. Ind. Appl.*, vol. IA-16, pp. 165-172, Mar./Apr. 1980.



Thomas M. Jahns (S'72-M'78) received the S.B. and S.M. degrees in 1974 and the Ph.D. degree in 1978 from the Massachusetts Institute of Technology, Cambridge, all in electrical engineering.

He joined Alexander Kusko Inc., Needham Heights, MA, in 1978 as a consulting engineer where he worked on power engineering projects in several areas including mass transportation and industrial drives. From 1979 to 1983 he worked at Gould Laboratories, Gould, Inc., in Rolling Meadows, IL. At Gould he participated in a variety of

programs developing new ac drive systems for both land and marine propulsion applications, as well as leading laboratory investigations of high-performance ac drives for industrial applications. In September 1983 he joined the General Electric Company at the Corporate Research and Development Center, Schenectady, NY, where he is pursuing research interests in variable-speed drive systems and power electronics.

Dr. Jahns is an active member of the IEEE-IAS Industrial Drives Committee and the recipient of two IEEE-IAS prize paper awards.